Inorganic Chemistry

pubs.acs.org/IC

Featured Article

Lowering the Symmetry of Cofacial Porphyrin Prisms for Selective Oxygen Reduction Electrocatalysis

Daoyang Zhang, Matthew R. Crawley, Amanda N. Oldacre, Lea J. Kyle, Samantha N. MacMillan, and Timothy R. Cook*

Cite This: *Inorg. Chem.* 2023, 62, 1766−1775

Read Online

ACCESS | Metrics & More | Article Recommendations | Supporting Information

ABSTRACT: Cofacial porphyrin catalysts for the Oxygen Reduction Reaction (ORR) formed via coordination-driven self-assembly have so far been limited to designs with fourfold symmetry, where four molecular clips bridge two porphyrin sites. We have synthesized six Py_nPh_m (Py = pyridyl, Ph = phenyl) metalloporphyrin prisms (Co^{2+}, Zn^{2+}) bridged by molecular clips containing two Rh^{3+} centers. Four of these structures are lower symmetry, with the Py_3Ph and Py_2Ph_2 prisms containing three and two molecular clips, respectively. The Co^{2+} species were evaluated for their ORR activity. Cyclic and hydrodynamic voltammetry studies of heterogeneous catalyst inks in aqueous media revealed marked differences in selectivity from ∼5% (Py_3Ph) to ∼37% (Py_2Ph_2) for the formation of H_2O_2. The single-crystal X-ray structure of the Zn_2 Py_2Ph_2 prism shows an offset between the porphyrin faces. This structural feature may be responsible for the change in selectivity, consistent with previous studies of covalently tethered cofacial porphyrins that have shown that geometry is a critical determinant of two-electron/two-proton versus four-electron/four-proton pathways. Extraction of standard rate constants k_s for the ORR revealed a cofacial enhancement of ∼2 orders of magnitude over mononuclear Co^{2+} tetrapyridyl porphyrin. Even though all the prisms described here use the same molecular clip, the resultant structures, and thus the reactivity for the ORR, differ significantly based on the number and orientation of pyridyl donor groups on the porphyrins, highlighting how coordination-driven self-assembly can be used to rapidly tune dinuclear catalysts.

INTRODUCTION

Molecular catalysts for the Oxygen Reduction Reaction (ORR) can be traced back to the pioneering work by Jasinski in 1964 on a cobalt phthalocyanine complex as the active component of a fuel cell run under basic conditions.[1] Over the next half-century, a wide library of molecular catalysts have been studied under aqueous and nonaqueous conditions, especially metal-containing N-macrocyclic complexes.[2] These studies have established that mononuclear systems often follow a two-electron/two-proton reduction to H_2O_2 either in addition to or exclusively over the four-electron/four-proton reduction to H_2O.[2] In fact, the original cobalt phthalocyanine catalyst was later measured to be ∼50% selective for hydrogen peroxide, and related systems can be as high as 98% selective under chemical reduction conditions for this two-electron/two-proton product.[3,4]

Challenges in the selectivity of catalysts for the ORR prompted explorations of dinuclear systems which often invoke biomimetic inspiration from cytochrome c oxidase as the basis for effective oxygen reduction.[5] There are three reasons why dinuclear metals may be better than their mononuclear counterparts. First, multielectron, multiproton inventories are more easily managed across two metal centers, which is a necessary requirement of many small-molecule activations, including the ORR. Second, both metals may participate in the binding of substrates and intermediates, which can lower energy barriers to afford faster kinetics. Third, if both metals can help stabilize a key intermediate of one reaction pathway over another, the selectivity may be greatly influenced. From the standpoint of studying the activity, these features may support lower overpotentials, higher faradaic efficiencies, and improved selectivities compared to mononuclear catalysts.[6−10]

That said, it is not a given that two metals will outperform a mononuclear catalyst. In fact, many cofacial systems still show significant H_2O_2 production, and it was not until the discovery of the Co_2 FTF4 architecture that a macrocyclic catalyst demonstrated direct four-electron/four-proton chemistry, with <10% selectivity for H_2O_2.[11] Related pillared architectures, where two porphyrins are linked through a single rigid covalent bridge, show similar selectivities that are sensitive to the nature

Special Issue: Discrete Coordination Cages and Metal Clusters

Received: April 1, 2022
Published: June 14, 2022

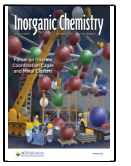

https://doi.org/10.1021/acs.inorgchem.2c01109
Inorg. Chem. 2023, 62, 1766−1775

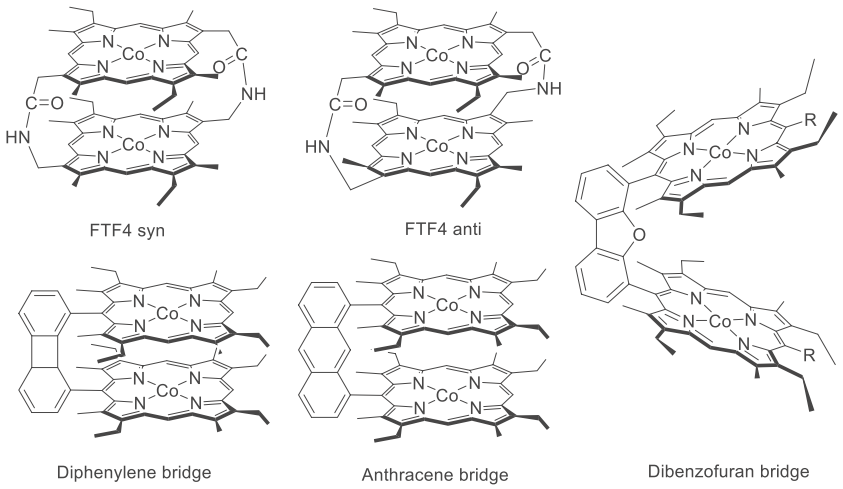

Figure 1. Literature-reported cofacial cobalt porphyrins for ORR catalysts.

of the bridge (<8% H_2O_2, diphenylene bridge; <15% H_2O_2, anthracene bridge;[12] ~28% H_2O_2, dibenzofuran bridge[13,14]), as shown in Figure 1. These pioneering studies of cofacial porphyrins implicate the stabilization of a μ-peroxo intermediate as a critical determinant of selectivity.[12]

Even with these impressive selectivities and compelling mechanistic studies, there remain many outstanding questions about how cofacial porphyrins carry out the ORR. Elucidating this reactivity requires systematic changes to both physical and electronic structure that may be difficult to achieve using covalent approaches that often involve multiple-step syntheses and multiple chromatographic purifications. These synthetic challenges and associated low yields have limited the library of cofacial architectures, which in turn hinders a deeper understanding of reactivity and mechanism.[15,16]

Our strategy to obtain cofacial catalysts for the ORR has been to exploit coordination-driven self-assembly[17−19] between pyridyl-functionalized porphyrins and so-called molecular clips that arrange two metals with offset and parallel coordination sites. When combined in solution, metal−ligand bond formation may drive the assembly of cofacial prisms (Scheme 1),[20] though

Scheme 1. Simple Illustration of the Coordination-Driven Self-Assembly of Cofacial Prisms and Various Kinetic Intermediates That May Form during the Assembly Process

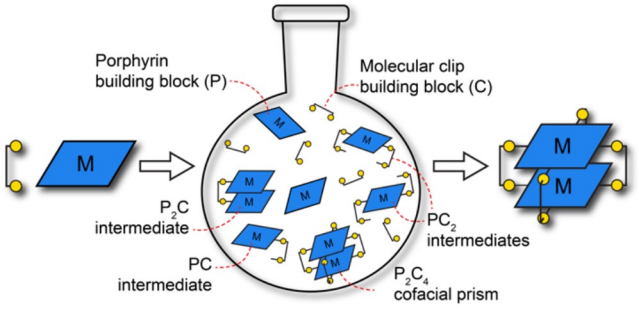

it is possible to form bowtie-like structures if the pyridyl sites on a single porphyrin are simply bridged[21] or more complex structures with other building blocks.[22,23] Our group demonstrated that when suitable metalloporphyrins are used, there is a significant cofacial kinetic enhancement for both chemical and electrochemical O_2 reduction.[24] We varied metal−metal separation to show changes to selectivity,[25] and we continued to tune the properties of these architectures through modification of the molecular clip building blocks.[26]

To date, the only examples of ORR by coordination-driven self-assembled catalysts have fourfold symmetry, requiring four molecular clips to bridge Py_4 meso-functionalized pyridyl porphyrins.[24−26] By changing the number of pyridyl groups, the stoichiometry of self-assembly necessarily changes, and herein we explore lower-symmetry prisms. We were particularly interested in *trans*-Py_2Ph_2 systems owing to similarities to the classic Co_2 FTF4 catalyst as well as Py_3Ph systems, since analogous "three-strapped" covalently tethered porphyrins have gone essentially unexplored over the past decades. As such, we carried out a one-pot reaction to generate statistical combinations of meso-functionalized phenyl and pyridyl porphyrins, enabling us to isolate Py_4, Py_3Ph, and *trans*-Py_2Ph_2 building blocks (Py = pyridyl, Ph = phenyl) for subsequent assembly with a rhodium-based molecular clip (Rhoxo clip)[27] to form Zn_2 and Co_2 prisms. The Co_2 prisms were evaluated as electrocatalysts for the ORR under homogeneous and heterogeneous conditions.

EXPERIMENTAL SECTION

Chemicals were purchased from commercial sources and used as received unless otherwise noted below. Solvents were purified using a solvent-drying system (Pure Process Technology). The rhodium-based molecular clip was prepared following a literature procedure.[27] ^{1}H NMR spectra were acquired on Varian 300, 400, or 500 MHz spectrometers. Chemical shifts (δ) are reported in parts per million (ppm) and referenced against the residual proton resonance of the deuterated solvent. Mass spectra were recorded on an electrospray ionization (ESI) linear ion trap (LTQ)-Orbitrap XL mass spectrometer (Thermo Fisher Scientific) or by electrospray ionization using a home-built sprayer into a Bruker SolariX 12 T FTMS (12 T FT-ICR) system equipped with a dual source. No precautions were taken to exclude air (O_2 or water) from self-assembly reactions.

One-Pot Synthesis of Tetrapyridyl-, Tripyridylphenyl-, and *trans*-Dipyridyldiphenyl Porphyrins. 4-Pyridinecarboxaldehyde (0.83 g, 7.5 mmol, 3.0 equiv) and benzaldehyde (0.25 g, 2.5 mmol, 1.0 equiv) were added to 50 mL of propionic acid. The mixture was brought to reflux while stirring. Freshly distilled pyrrole (0.67 g, 10. mmol, 4.0 equiv) was then added dropwise over the course of 30 min. The final mixture was further refluxed for an additional 60 min after which it was allowed to cool to room temperature and the solvent volume reduced to half in vacuo. The cooled and reduced solution was placed in a 5 °C refrigerator for 30 min. The solid that formed was

https://doi.org/10.1021/acs.inorgchem.2c01109
Inorg. Chem. 2023, 62, 1766−1775

collected by filtration and washed with cold methanol (3 × 20 mL) and dried under vacuum to afford a crude purple solid. The crude product contained all three desired porphyrins, and these were further separated by column chromatography on silica gel with dry loading, initially using 100:1 chloroform/methanol and transitioning to a 20:1 eluent. We note that in addition to the Py_4, Py_3Ph, and *trans*-Py_2Ph_2 porphyrins, the crude product also contained other variants (e.g., Ph_4, Ph_3Py, and *cis*-Py_2Ph_2.). The greater the number of pyridyl groups, the slower a given porphyrin eluted, facilitating separation and isolation (*trans*-Py_2Ph_2 first, Py_3Ph second, Py_4 last).

General Metalation Procedure. A mixture of free-base porphyrin (100 mg, 0.16 mmol, 1.0 equiv) and $M(OAc)_2$ (M = Co, Zn) (0.64 mmol, 4.0 equiv) in DMF was refluxed for 5 h. The reaction mixture was poured into water to precipitate a crystalline product, which was filtered and washed with water (3 × 10 mL) and then ethanol (3 × 10 mL) and then characterized by ESI-LTQ-MS. Zn Py_3Ph: $(M + H^+)$ m/z = 680.150. Zn Py_2Ph_2: $(M + H^+)$ m/z = 679.160. Co Py_3Ph: $(M + H^+)$ m/z = 674.227. Co Py_2Ph_2: $(M + H^+)$ m/z = 673.146 (as shown in Figures S17−S20).

General Self-Assembly Procedure. The stoichiometry of porphyrin, Rhoxo clip, and AgOTf used in self-assembly reactions was dictated by the number of pyridyl groups. For Py_4 prisms, 4.0 equiv of the chloro-ligated molecular clip was combined with 2.0 equiv of tetrapyridyl porphyrin in the presence of 8.8 equiv of AgOTf. For the Py_3Ph prisms, 3.0 equiv of the chloro-ligated molecular clip was combined with 2.0 equiv of tripyridylphenyl porphyrin in the presence of 6.6 equiv of AgOTf. For the Py_2Ph_2 prisms, 2.0 equiv of the chloro-ligated molecular clip was combined with 2.0 equiv of tetrapyridyl porphyrin in the presence of 4.4 equiv of AgOTf. Self-assembly was achieved by first combining a quantity of chloro-ligated Rhoxo clip with AgOTf in 10 mL of methanol with the exclusion of light. This solution was stirred for 3 h, prompting the formation of AgCl which was removed via filtration through a pipet plugged with glass fiber. The filtrate was added directly to a suspension of the desired porphyrin in 5 mL of methanol. This final mixture was refluxed for 48 h upon which it was cooled and filtered once more through a pipet plugged with glass fiber to remove any insoluble byproducts, and the remaining solvent was removed by rotary evaporation. The crude product was recrystallized by dissolution in methanol and the addition of diethyl ether. Purified cofacial prisms were dried under vacuum for at least 12 h prior to spectroscopic or electrochemical analysis.

*Self-Assembly of the **Zn_2 Py_4 Prism**.*

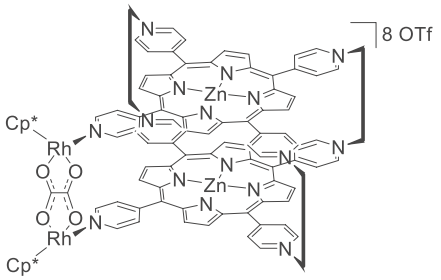

Rhoxo clip (41.31 mg, 0.065 04 mmol, 4.000 equiv), AgOTf (34.09 mg, 0.1327 mmol, 8.160 equiv), and ZnTPyP (22.16 mg, 0.032 49 mmol, 1.998 equiv) in 12.0 mL of methanol. Yield: 62.37 mg (0.013 00 mmol) of the **Zn_2 Py_4 Prism**, 80.00%. ^{1}H NMR (500 MHz, CD_3OD) δ 9.02 (d, J = 5.6 Hz, 8H pyridyl), 8.92 (d, J = 4.6 Hz, 8H pyrrolic), 8.89 (d, J = 4.6 Hz, 8H pyrrolic), 8.54 (d, J = 5.5 Hz, 8H pyridyl), 8.49 (dd, J = 5.8, 2.2 Hz, 8H pyridyl), 8.08 (dd, J = 5.6, 2.2 Hz, 8H pyridyl), 1.93 (s, 120H Cp*). UV−vis (MeOH): soret band λ_{max} = 422 nm, Q bands λ_{max} = 556, 596 nm.

*Self-Assembly of the **Co_2 Py_4 Prism**.*

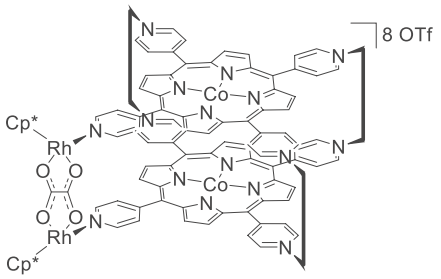

Rhoxo clip (41.14 mg, 0.064 77 mmol, 4.000 equiv), AgOTf (33.83 mg, 0.1317 mmol, 8.131 equiv), and CoTPyP (21.80 mg, 0.032 27 mmol, 1.993 equiv) in 12.0 mL of methanol. Yield: 49.77 mg (0.010 37 mmol) of the **Co_2 Py_4 Prism**, 64.28%. UV−vis (MeOH): soret band λ_{max} = 415 nm, Q-band λ_{max} = 535 nm.

*Self-Assembly of the **Zn_2 Py_3Ph Prism**.*

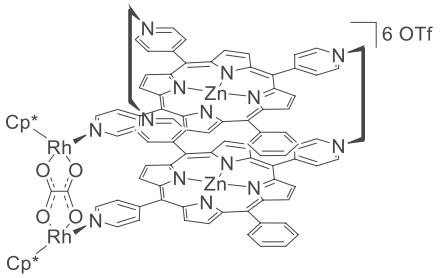

Rhoxo clip (10.0 mg, 0.0158 mmol, 3.00 equiv), AgOTf (9.09 mg, 0.0354 mmol, 6.60 equiv), and Zn Py_3Ph porphyrin (7.15 mg, 0.0105 mmol, 2 equiv) in 15 mL of methanol. Yield: 15.2 mg (0.003 86 mmol) of the **Zn_2 Py_3Ph Prism**, 73.4%. ^{1}H NMR (500 MHz, CD_3OD): δ = 9.28−7.44 (m, 50H; pyrrole, pyridyl, phenyl Ar−H), 2.00−1.80 (m, 90H; Cp* CH_3). UV−vis (MeOH): soret band λ_{max} = 421 nm, Q-band λ_{max} = 556 nm, 596 nm.

*Self-Assembly of the **Co_2 Py_3Ph Prism**.*

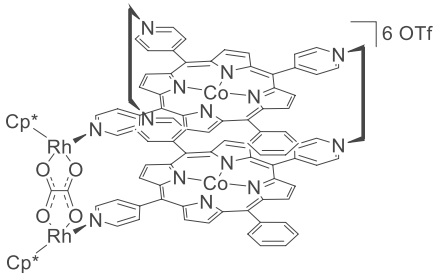

Rhoxo clip (10.0 mg, 0.0158 mmol, 3.00 equiv), AgOTf (9.09 mg, 0.0354 mmol, 6.60 equiv), and Co Py_3Ph porphyrin (7.17 mg, 0.0105 mmol, 2 equiv) in 15 mL of methanol. Yield: 13.4 mg (0.00340 mmol) of the **Co_2 Py_3Ph Prism**, 64.7%. UV−vis (MeOH): soret band λ_{max} = 416 nm, Q-band λ_{max} = 535 nm.

*Self-Assembly of the **Zn_2 Py_2Ph_2 Prism**.*

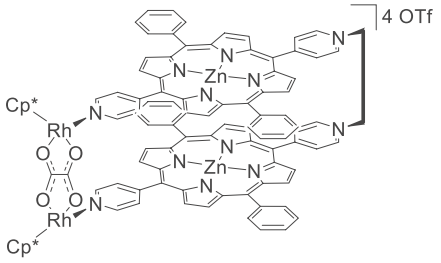

Rhoxo clip (10.0 mg, 0.0158 mmol, 2.00 equiv), AgOTf (9.09 mg, 0.0354 mmol, 4.40 equiv), and Zn Py_2Ph_2 porphyrin (10.7 mg, 0.0158 mmol, 2 equiv) in 15 mL of methanol. Yield: 20.3 mg (0.000 658 mmol) of the **Zn_2 Py_2Ph_2 Prism**, 83.5%. ^{1}H NMR (500 MHz, CD_3OD): δ = 9.20−8.76 (m, 26H; pyrrole, pyridyl, phenyl Ar−H), 8.76−858 (m, 10H; pyrrole, pyridyl, phenyl Ar−H), 8.45−8.04 (m,

https://doi.org/10.1021/acs.inorgchem.2c01109
Inorg. Chem. 2023, 62, 1766−1775

Scheme 2

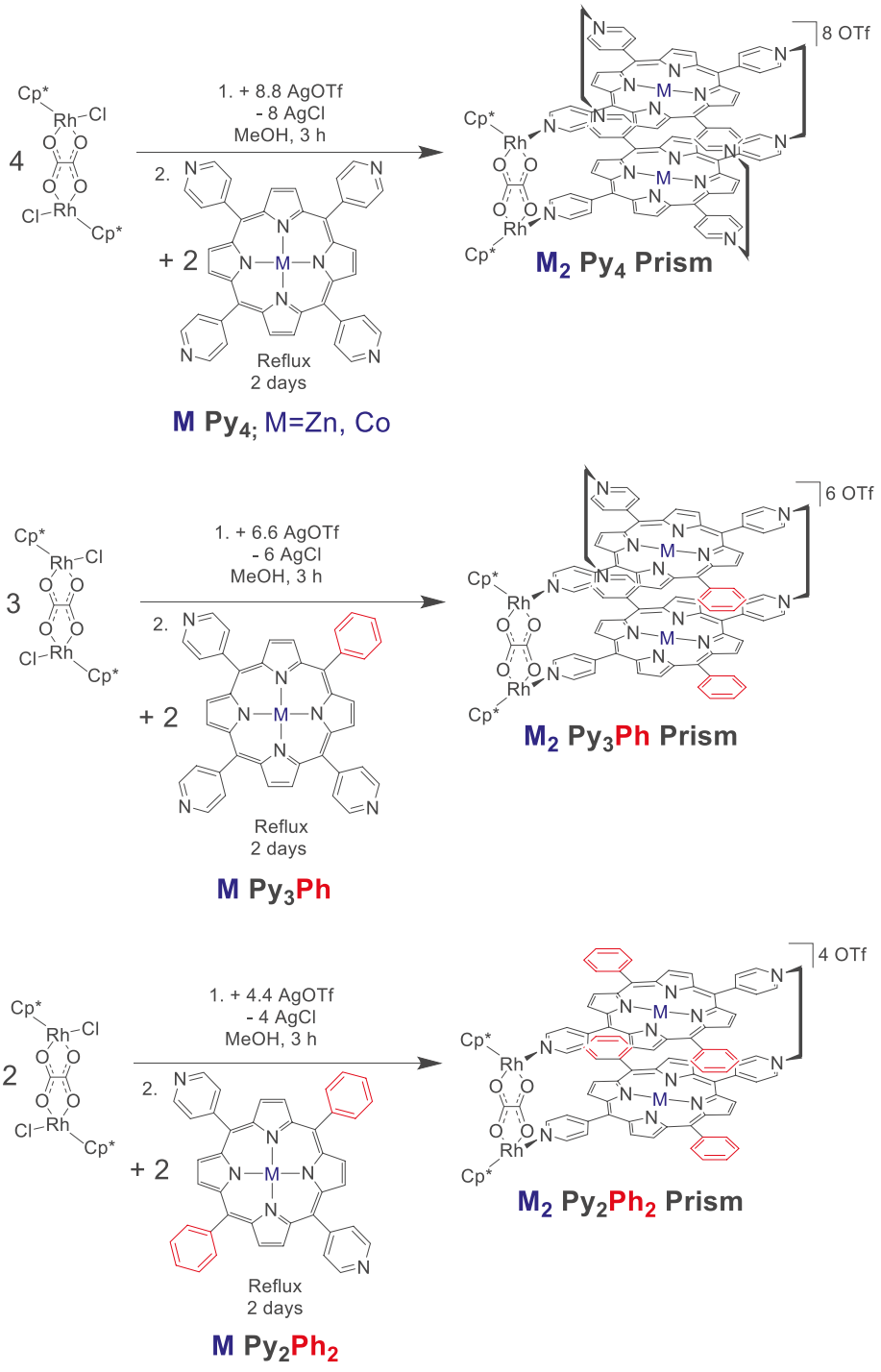

16H; pyrrole, pyridyl, phenyl Ar−H), 1.92 (s, 60H; Cp* CH_3). UV−vis (MeOH): soret band λ_{max} = 422 nm, Q-band λ_{max} = 558, 596 nm.

Self-Assembly of the ***Co_2 Py_2Ph_2 Prism.***

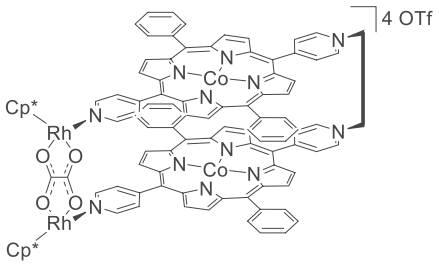

Rhoxo clip (10.0 mg, 0.0158 mmol, 2.00 equiv), AgOTf (9.09 mg, 0.0354 mmol, 4.40 equiv), and Co Py_2Ph_2 porphyrin (10.6 mg, 0.0158 mmol, 2 equiv) in 15 mL of methanol. Yield: 15.3 mg (0.004 98 mmol) of the **Co_2 Py_2Ph_2 Prism**, 63.2%. UV−vis (MeOH): soret band λ_{max} = 416 nm, Q-band λ_{max} = 535 nm.

Electrochemical Analysis. All electrochemical experiments were performed using a BioLogic SP-300 bipotentiostat. $TBAPF_6$ was recrystallized three times from ethanol and dried for at least 48 h in vacuo before use in nonaqueous experiments. Acetonitrile was dried using a Pure Process Technology solvent system. Cyclic voltammograms (CVs) under homogeneous conditions were carried out in acetonitrile with 100 mM concentration of $TBAPF_6$ as a supporting electrolyte. A glassy carbon working electrode (3 mm diameter) and a

https://doi.org/10.1021/acs.inorgchem.2c01109
Inorg. Chem. 2023, 62, 1766−1775

Pt wire counter electrode were used. A nonaqueous $Ag/AgNO_3$ reference electrode was used. At the completion of experiments, ferrocene was added to the cell to convert all nonaqueous potentials to Fc^+/Fc.

For heterogeneous films in aqueous media, nanopore water was used to prepare 0.5 M H_2SO_4 solutions, which served as both the proton source as well as the electrolyte. A glassy carbon working electrode (3 mm) and a Pt wire counter electrode were used. The reference was an aqueous Ag/AgCl (3 M KCl) electrode.

For hydrodynamic voltammetry, a Pine MSR rotator was used with a glass carbon disk, Pt ring, and ring-disk electrode. Scan rates were 100 mV/s for CVs and 20 mV/s for linear sweep voltammograms. Selectivities were determined by holding the ring at a 1.0 V potential to reoxidize any H_2O_2 that formed. The collection efficiency of the RRDE electrode was established using $K_3Fe(CN)_6$ to enable the use of eq 1.

$$\%\ H_2O_2 = \frac{\frac{2i_{ring}}{N}}{i_{disk} + \frac{i_{ring}}{N}} \times 100 \quad (1)$$

Catalyst ink film preparation: In a 2-dram vial, 1.0 μmol of catalyst, 5.5 mg of carbon black, 100 μL of ethanol, and 500 μL of methanol were sonicated for 1 h. The solvent was then evaporated in vacuo, followed by the addition of a 70 μL Nafion solution (5% w/w in isopropyl alcohol) and 600 μL of ethanol, and the suspension was sonicated for 1 h. The Nafion catalyst ink was then pipetted onto the working electrode. When CVs were acquired using a 3 mm working electrode, 2 μL was drop cast onto the surface and allowed to stand in air until dry. In the case of the larger glassy carbon disk for the ring-disk electrode, 3 μL was used to completely cover the surface.

Crystallography. Single crystals of the **Zn_2 Py_4 Prism** were grown by vapor diffusion of diethyl ether into a solution of the prism in CH_2Cl_2. Crystals were small, red, cubic blocks (0.06 × 0.06 × 0.08 mm^3). The datum crystal was mounted on a glass fiber, and the data was collected on a Bruker-APEXII diffractometer, with a Mo rotating anode, and a APEXII area detector at 100 K. Even with 120 s exposures, diffraction intensities beyond 1.2 Å were not measurable. This is not uncommon for crystals of these architectures. A series of ω-scans were used to cover reciprocal space. Beyond weak diffraction, the first evidence of a problematic structure was the difficulty associated with data indexing. Indexing was performed using APEX3, and several possible unit cells were found.[28] Ultimately, a tetragonal cell was selected and used in data reduction. Integration and scaling were also performed in the APEX3 software package. The space group was found to be $P422$; the assignment was made on the basis of E^2 statistics and the successful refinement of the structure. Structure solution was performed using SHELXT[29] via intrinsic phasing, and least-squares refinement was done with SHELXL[30] in the Olex2 (ver. 1.5) software package.[31]

The structure refinement of the **Zn_2 Py_4 Prism** was notably challenging. The asymmetric unit consisted of 1/8th of a formula unit, along with numerous solvent/triflate counterions. Attempts at modeling the solvent and counterions were ineffective. The crystal exhibited a layered structure with alternating layers of prisms and heavily disordered solvent and counterions. After all other options to model at the very least the counterions were exhausted, a solvent mask was applied in Olex2 to address the disordered layers. A single void space of 7732 $Å^3$ was found which contained 1907 e^- per unit cell. On the basis of the charge neutrality and the number of electrons, we assigned the contents of the void space to 8 triflate anions and 32 CH_2Cl_2 solvent molecules. These sum to 1928 e^- per unit cell, in good agreement with the number of electrons found by the solvent mask. We have elected to assign the entire void space to be CH_2Cl_2; however, we cannot rule out the possibility, and indeed likelihood, that diethyl ether also contributes to the disordered solvent layers. Nevertheless, this does not detract from the final conclusion that the desired cofacial architecture has indeed been synthesized in the expected confirmations and stoichiometry.

Single crystals of the **Zn_2 Py_2Ph_2 Prism** were grown by the slow evaporation of methanol. Crystals were red blocks. The crystal (0.071 × 0.168 × 0.233 mm^3) was mounted on a Rigaku XtaLAB Synergy diffractometer coupled to a Rigaku Hypix detector with Cu Kα radiation (λ = 1.541 84 Å) from a PhotonJet microfocus X-ray source at 100 K. The diffraction images were processed and scaled using the CrysAlisPro software.[32] Structure solution and refinement were performed as outlined above for the **Zn_2 Py_4 Prism**.

The refinement of the **Zn_2 Py_2Ph_2 Prism** was significantly more straightforward than that of the **Zn_2 Py_4 Prism**. The prism crystallized in $P2_1/c$ with two half-fragments in the asymmetric unit. The first fragment showed no disorder, while the second showed disorder in one of the Rhoxo molecular clips and its corresponding pyridyl group. Specifically, a rocking motion led to positional disorder over two positions. The occupancy was allowed to freely refine and adopted a 70:30 ratio. Of the four expected counterions, two were found in the electron density map, while the other two remained disordered in the solvent accessible void space. Attempts to model the remaining two triflate counterions were unsuccessful, so a solvent mask was applied. Two independent voids were found with volumes of 2690 and 168 $Å^3$ containing 26 and 930 e^- per unit cell, respectively. The larger void was assigned 8 triflates anions and 20 methanol molecules per unit cell (944 e^-), and the smaller 1.32 methanol molecules (24 e^-). With Z = 4 and Z' = 1, the two triflates in the asymmetric unit correspond to 8 per unit cell; this totals the expected 16 anions per unit cell necessary for charge neutrality.

RESULTS AND DISCUSSION

Synthesis and Structural Characterization. These self-assembly reactions proceeded as expected for metal−pyridyl-based self-assemblies. Chloride is often problematic for such architectures as it can displace metal−pyridyl bonds, and so its removal using a standard AgOTf salt metathesis enabled clean self-assembly of all six porphyrin prisms as illustrated in Scheme 2. All six assemblies occurred with relatively high isolated yields, spanning 60−84%. We note that for the Py_4 assembly, if reactions are carried out in a sealed NMR tube, the only significant species observed in the ^1H NMR is the prism as shown in Figure 2. DOSY spectra of the crude reaction mixtures also support clean and near quantitative assembly as only a single diffusion is observed for all nonsolvent peaks (Figure S8).

Although the Co_2 prisms are paramagnetic and thus NMR information is of limited value, the Zn_2 analogues could be fully characterized by ^1H NMR to support symmetry and purity, along with DOSY NMR to gain information about the number of species in solution. In all cases, ^1H NMR was consistent with

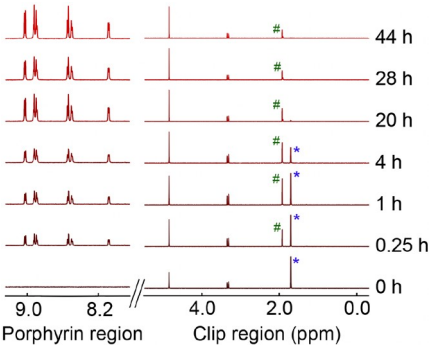

Figure 2. Time-evolution of the self-assembly of the **Zn_2 Py_4 Prism** monitored by ^1H NMR in a J-Young tube (CD_3OD, 500 MHz). Peak intensities of the porphyrin region are scaled independently from the clip region. * corresponds to Cp* in the free molecular clip, and # is the analogous Cp* resonance for the prism.

https://doi.org/10.1021/acs.inorgchem.2c01109
Inorg. Chem. 2023, 62, 1766−1775

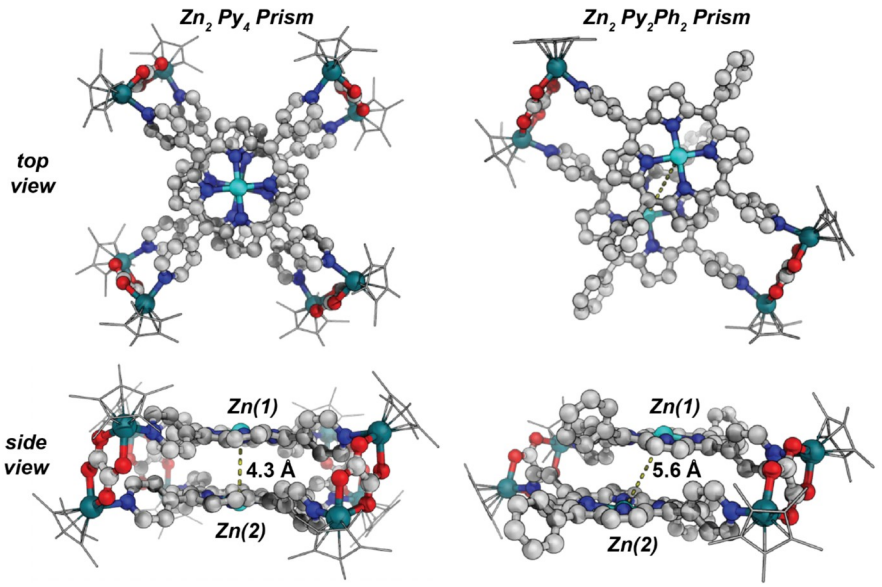

Figure 3. Single-crystal structures of the **Zn_2 Py_4 Prism** (left) and the **Zn_2 Py_2Ph_2 Prism** (right) illustrating the cofacial porphyrin arrangement and the effect of twisting and offset of the porphyrin planes on the metal−metal separation. Solvent molecules, counterions, and H atoms omitted for clarity.

our anticipated cofacial porphyrin architectures being octarhodium (Py_4 prisms), hexarhodium (Py_3Ph prisms), or tetrarhodium (Py_2Ph_2 prisms). The resonances corresponding to protons on the Cp* occur between 1 and 2 ppm; the resonances associated with pyridyl-, phenyl-, and pyrrolic-protons occur between 7.5 and 10 ppm. The high symmetry of the Py_4 prism results in well-resolved peaks and a relatively simple overall spectrum. The features corresponding to the α- and β-protons of the pyridyl groups, which are iconic in metal−pyridyl coordination-driven self-assemblies, can be seen clearly but are more complex in the Py_3Ph and Py_2Ph_2 prisms owing to their reduced symmetries. The Py_3Ph and Py_2Ph_2 structures break the symmetry of the pyridyl protons, so additional peaks and splitting are observed (see Figures S4 and S5). For all three Zn_2 prisms, every peak aside from those from solvents show the same diffusion, consistent with all protons being found on the same size species (DOSY NMRs, Figures S7−S10). Whereas NMR establishes purity and provides information about symmetry, ESI-MS is commonly used to investigate the stoichiometry of self-assembly since it is often possible to detect peaks that correspond to intact architectures that are charged by virtue of the loss of counterions. Indeed, for all six prisms, we find peaks that support our structural assignments of four, three, and two-clipped cofacial porphyrins for Py_4, Py_3Ph, and Py_2Ph_2, respectively (Figures S11−S16).

Crystallography. Single crystals suitable for X-ray diffraction were successfully grown for both the **Zn_2 Py_4** and **Zn_2 Py_2Ph_2** prisms (Figure 3). The observed structure of the former matches what we would anticipate from earlier syntheses of related architectures.[26] Two porphyrins are held in a cofacial arrangement, bridged by four molecular clips. The two Zn^{2+} metal centers are separated by a distance of 4.33 Å and reside on the crystallographic fourfold rotation axis. The planes generated by the pyrrolic N atoms are 3.88 Å apart, suggesting that the Zn^{2+} cations pucker ~0.23 Å above the plane of the porphyrin N atoms. The Zn^{2+} coordination environment can best be described as distorted square pyramidal. Four pyridyl N-donors and a single O-donor from either a poorly resolved axial methanol or water molecule complete the coordination sphere. The twist angle between the upper and lower porphyrin rings is 13.3°, resulting in a shortening of the M—M separation from the theoretical maximum of 5.57 Å based on the Rh−Rh distance in the molecular clip and a 0° twist angle.

Single crystals of the **Zn_2 Py_4 Prism** were twinned, and the inversion matrix was successfully used to relate the two twin domains (i.e., a racemic twin). This confirms that both helical isomers (*M* and *P*) were present in the crystal. The batch scale factor was refined to 0.50(5) indicating essentially equal contributions from each domain. Visualizing the packing of the crystal revealed a layered structure, wherein there are alternating layers of ordered cofacial prisms and disordered solvent and triflate counterions. The layers of highly disordered solvent and counterions help to explain the generally poor diffraction and the diffuse scattering observed in the *h*0*l* and 0*kl* precession images (see the Supporting Information). The precession image in the *hk*0 plane clearly illustrates the fourfold symmetry of the lattice and lacks strong diffuse scattering, indicative of the long-range ordering of the prism units down the crystallographic *c*-axis. The observed diffraction is similar to that of other layered structures in the literature.[33]

Descending from four molecular clips to two results in a dramatic change in the orientation of the porphyrins. The Zn-centers of the **Zn_2 Py_2Ph_2 Prism** were found to adopt a "slipped" conformation where the porphyrin units were laterally offset in space, rather than the coaxial configuration observed for the **Zn_2 Py_4 Prism**. The unit cell was found to have four formula units (Z = 4), with Z' = 1; however, instead of one full formula unit, we found two independent half-formula units. As such, there are two measurable Zn−Zn distances, 5.647 and 5.592 Å, the latter corresponding to the formula unit with the disordered clip. The larger Zn−Zn distance results from a different tilting motif in the molecular clip.

Electrochemical Analysis. Cofacial porphyrins are known to catalyze two pathways of oxygen reduction: the four-electron/four-proton reaction to generate water (eq 2) and the two-electron/two-proton reaction to form hydrogen peroxide (eq 3):

https://doi.org/10.1021/acs.inorgchem.2c01109
Inorg. Chem. 2023, 62, 1766−1775

$$4H^+ + 4e^- + O_2 \rightarrow 2H_2O;\ E^0 \text{ vs SHE} = 1.23\ \text{V} \quad (2)$$

$$2H^+ + 2e^- + O_2 \rightarrow H_2O_2;\ E^0 \text{ vs SHE} = 0.69\ \text{V} \quad (3)$$

The general mechanisms for the ORR by existing systems tend to invoke oxygen binding to either a Co_2(II, II) core[34] or a Co_2(III, II) core.[35] When subjected to reducing potentials in the presence of protons, these systems turn over with selectivities that vary, implicating metal−metal separation and structural rigidity as critical factors. We were thus interested in exploring the redox behavior of our lower symmetry Co_2 prisms and began our investigations with homogeneous CV experiments.

As shown in Figure 4, all three Co_2 prisms show negligible background current in the absence of both O_2 and trifluoroacetic

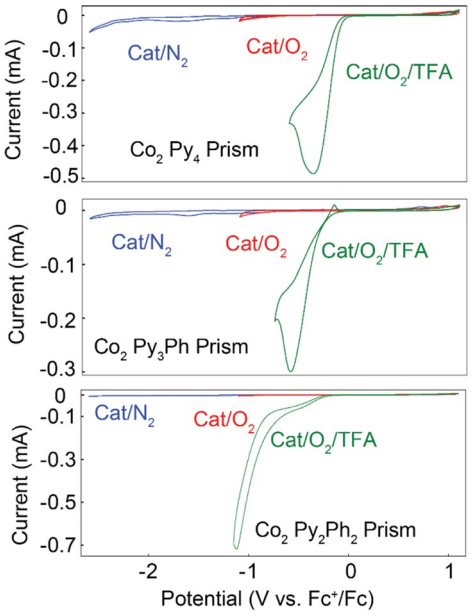

Figure 4. CVs of Co_2 prisms under homogeneous conditions. Blue: 0.1 mM prism, N_2 atmosphere; red: 0.1 mM prism, O_2 atmosphere; green: 0.1 mM prism, O_2 atmosphere, 100 mM TFA. In all cases, dry acetonitrile with 100 mM $TBAPF_6$ was used. Scan rate: 100 mV/s.

acid, which we used as a proton source in our nonaqueous experiments. The noncatalytic features are shown in more detail in Figures S22 and S23, where complex reduction events associated with porphyrin and clip-centered redox chemistry occur. When these catalysts are subjected to potentials below 0 V vs Fc^+/Fc, a large current response is observed which we ascribe to catalytic O_2 reduction. To confirm that the ORR catalysis was occurring because of the Co_2 cores and not a different self-assembly component, CV experiments were also carried out with the Zn_2 analogues under the same conditions. No catalytic responses were observed for all three Zn_2 species. We note that the catalytic response does differ between the Co_2 prisms, with the **Co_2 Py_4 Prism** and the **Co_2 Py_3Ph Prism** exhibiting more positive $E_{cat/2}$ values relative to the **Co_2 Py_2Ph_2 Prism**, though all three prisms show similar onset potentials.

To further explore the reactivity of the Co_2 prisms for the ORR, we immobilized the catalysts in an ink of Nafion and carbon which enabled the fabrication of heterogeneous electrodes on glassy carbon disks for experiments to extract faradaic efficiencies and kinetic information. The CVs of these inks are shown in Figure 5, run under aqueous conditions with 0.5 M H_2SO_4 as a proton source and as a supporting electrolyte.

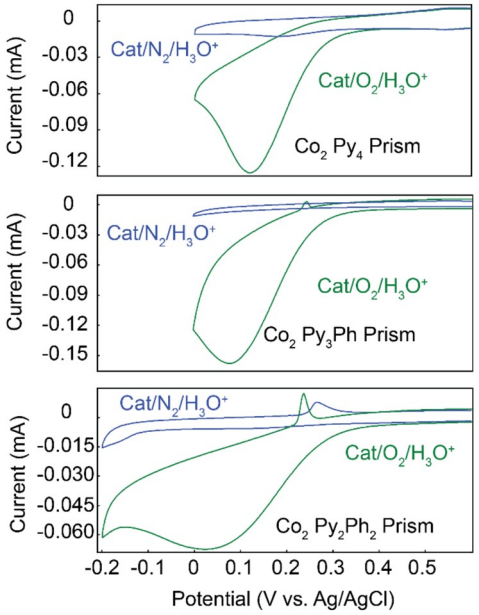

Figure 5. CVs of Co_2 prisms under heterogeneous conditions. Blue: N_2 atmosphere; green: O_2 atmosphere. Catalysts were immobilized in Nafion inks with carbon black and immersed in 0.5 M H_2SO_4. Oxygen gas was bubbled through the solution to saturate it before each data collection. Reference electrode: AgCl in 3 M KCl. Scan rate: 100 mV/s.

In the absence of O_2, no catalytic current response is observed, nor is there any evidence of proton reduction in the potential ranges of interest. When the solutions were sparged with O_2, the CVs of all three prisms show clear current response that is consistent with oxygen reduction. We observe a similar trend to the homogeneous experiments, where all three prisms have similar onset potentials, but the **$Co_2Py_2Ph_2$ Prism** has a more negative $E_{cat/2}$.

To establish the selectivity of these catalysts for the ORR, rotating-ring disk electrode (RRDE) studies were carried out. The ring and disk currents measured for the three prisms collected at 2500 rpm are shown in Figure 6. These current responses were used to calculate the faradaic efficiency of H_2O_2 production, which are shown in the lower plot of Figure 6. In addition to the prisms, we measured the selectivity of cobalt tetrapyridyl porphyrin (CoTPyP), which formed ∼60% H_2O_2, consistent with our previous investigations.[25] All three prisms showed a significant enhancement in selectivity relative to CoTPyP, where the two-electron/two-proton pathway is clearly suppressed. The most selective of the prisms was the **Co_2 Py_3Ph Prism**, which had an H_2O_2 faradaic efficiency of 4.6% taken as the average across all applied potentials. The **Co_2 Py_4 Prism** also strongly favors four-electron/four-proton chemistry, with an average of 15% H_2O_2. The selectivity of the slipped **Co_2 Py_2Ph_2 Prism** for H_2O_2 is notably higher, averaging 35% across all applied potentials. Since the Co_2 prism is expected to be isostructural with the Zn_2 analogue, we ascribe this difference in selectivity to the slipped or offset arrangement of the porphyrin faces. There is some precedent for this as the selectivities of Co_2 FTF4 and alkyl-modified variants, which have essentially coaxial metalloporphyrins, are <10% H_2O_2, but when "slipped" versions are made where the metals are offset, the % H_2O_2 skyrockets to 80−85%.[36] The long-standing explanation for this effect is that the nature of Co−O−O−Co binding within the cofacial cleft determines if subsequent proton and electron transfer results in

https://doi.org/10.1021/acs.inorgchem.2c01109
Inorg. Chem. 2023, 62, 1766−1775

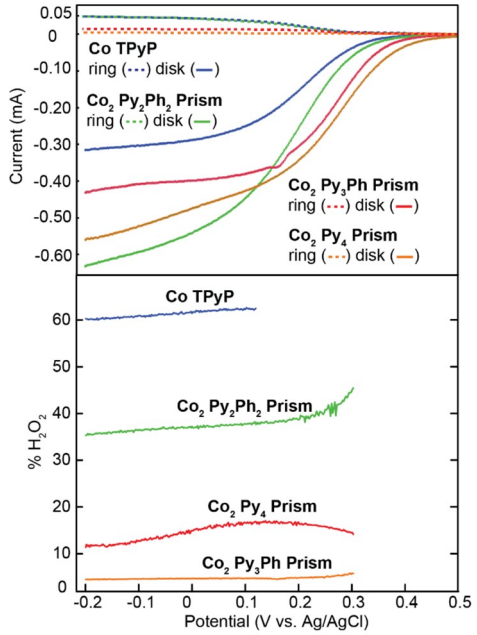

Figure 6. Hydrodynamic voltammograms of the three Co_2 prisms using RRDE at scan rates of 20 mV/s (top). Selectivities of the three prisms and CoTPyP based on the faradaic efficiency of H_2O_2 generation in 0.5 M H_2SO_4 at 2500 rpm (bottom).

cleavage of the O−O bond, necessary to generate water, or not, resulting in hydrogen peroxide. A rigid coaxial geometry favors cis binding, whereas an offset geometry favors trans binding.[36] Proposed mechanisms differ in the literature. Some summaries invoke a Co(III)−O−O−Co(III) μ-superoxo as the key species that can either be protonated to favor the H_2O pathway or reduced to the μ-peroxo for the H_2O_2 pathway.[35] Other pathways still complete four-electron, four-proton cycles from the μ-peroxo.[34] That said, it is clear that a cofacial cleft is not an absolute requirement for four-electron chemistry, and related monomeric systems are emerging that are significantly selective for water, as demonstrated recently with isocorroles.[37]

In addition to measuring faradaic efficiencies, we subjected our heterogeneous catalyst inks to Koutecký−Levich analyses of the ORR to ultimately determine standard rate constants (k_s). These results are summarized in Table 1. When the heterogeneous inks were prepared, the amount of CoTPyP added to the mixture was twice the amount of the prisms, so that the number of Co sites was kept constant in all materials. Thus, any changes to kinetics are ascribed to cofacial enhancements and not because there are two cobalt sites per prism. The standard rate constants of all three prisms are 2 orders of magnitude greater than that of the monomeric CoTPyP. Among the prisms, the k_s values are all similar in magnitude. On the one hand, this suggests that the slipped geometry of the **Co_2 Py_2Ph_2 Prism**, which had such a notable influence on selectivity, does not manifest in significantly different kinetics. On the other hand, because the selectivities are so different, the standard rate constant for this low-symmetry prism has contributions from the two-electron/two-proton pathway that are not captured to nearly the same degree in the current response of the **Co_2 Py_3Ph Prism**, for which the four-electron/four-proton pathway dominates. Thus, although it is fair to say that the kinetics are similar, there is no way to decouple the two pathways to compare rate constants exclusively for water production. Nonetheless, because the **Co_2 Py_3Ph Prism** has the largest standard rate constant and is most selective for the more challenging four-electron/four-proton pathway, this prism is highly effective in catalyzing the ORR. Maintaining a coaxial Co−Co arrangement along with opening up one of the clipped sites has a clear influence.

Table 1. Parameters of Co_2 Prism Inks Determined by Electrochemical Analyses

prism	$E_{cat/2}$ (V vs Ag/AgCl)	E_{onset} (V vs Ag/AgCl)	N_{app}[a]	% H_2O_2	% H_2O[b]	k_s[c] (M^{-1} s^{-1})
Co_2 Py_4	0.24	0.39	3.7	14.5%	85.5%	$2.3(2) \times 10^2$
Co_2 Py_3Ph	0.27	0.40	3.9	4.6%	95.4%	$2.6(2) \times 10^2$
Co_2 Py_2Ph_2	0.20	0.32	3.3	37.2%	62.8%	$2.0(3) \times 10^2$
CoTPyP	0.14	0.28	2.8	61.3%	38.7%	$3.5(3) \times 10^0$

[a]Determined based on the following equation: $N_{app} = 4 - 2\frac{(\% H_2O_2)}{100}$. [b]100 − % H_2O_2. [c]Determined based on the following equation: $i_k = nFAk_{het}[O_2]\Gamma_{cat}$.

CONCLUSION

We have expanded the library of self-assembled cofacial porphyrins to include two-clipped and three-clipped architectures capable of catalyzing the ORR. The Zn_2 variants were used to aid in structural characterization, which helped to establish that the prisms formed from Py_3Ph porphyrins were structurally rigid with coaxial cofacial arrangements whereas the Py_2Ph_2 analogues adopted slipped geometries where the two porphyrin faces were offset. Our coordination-driven self-assembly approach enabled us to form these species in high isolated yields of 60−84% with evidence of near quantitative assembly in solution. The Co_2 prisms were evaluated as electrocatalysts for the ORR, revealing cofacial enhancements to both kinetics and selectivity over mononuclear CoTPyP. The strength of the cofacial effects differs with the geometry/stoichiometry of self-assembly, most notably for H_2O_2 selectivity, with the **Co_2 Py_3Ph Prism** forming only ∼5% of this two-electron/two-proton product. Although there is a notable enhancement to the standard rate constants for each prism, the differences between the prisms are minor. Work is underway to better understand these cofacial effects and the mechanism of the ORR in these self-assembled catalysts, especially in the context of how O_2 binds (within the cofacial cleft or to an external face) and if key reduced intermediates may be characterized.

ASSOCIATED CONTENT

Supporting Information

The Supporting Information is available free of charge at https://pubs.acs.org/doi/10.1021/acs.inorgchem.2c01109.

^{1}H NMR and DOSY NMR, ESI-MS, cyclic voltammograms, LSV, RDE, and crystallography data tables (PDF)

Accession Codes

CCDC 2161516 and 2161548 contain the supplementary crystallographic data for this paper. These data can be obtained free of charge via www.ccdc.cam.ac.uk/data_request/cif, or by emailing data_request@ccdc.cam.ac.uk, or by contacting The Cambridge Crystallographic Data Centre, 12 Union Road, Cambridge CB2 1EZ, UK; fax: +44 1223 336033.

https://doi.org/10.1021/acs.inorgchem.2c01109
Inorg. Chem. 2023, 62, 1766−1775

AUTHOR INFORMATION

Corresponding Author

Timothy R. Cook − *Department of Chemistry, University at Buffalo, The State University of New York, Buffalo, New York 14260, United States*; Email: trcook@buffalo.edu

Authors

Daoyang Zhang − *Department of Chemistry, University at Buffalo, The State University of New York, Buffalo, New York 14260, United States*; orcid.org/0000-0003-3722-1336

Matthew R. Crawley − *Department of Chemistry, University at Buffalo, The State University of New York, Buffalo, New York 14260, United States*; orcid.org/0000-0002-2555-9543

Amanda N. Oldacre − *Department of Chemistry, University at Buffalo, The State University of New York, Buffalo, New York 14260, United States*; Present Address: Department of Chemistry, St. Lawrence University, Canton, NY 13617; orcid.org/0000-0001-8873-7186

Lea J. Kyle − *Department of Chemistry, University at Buffalo, The State University of New York, Buffalo, New York 14260, United States*

Samantha N. MacMillan − *Department of Chemistry and Chemical Biology, Cornell University, Ithaca, New York 14853, United States*

Complete contact information is available at: https://pubs.acs.org/10.1021/acs.inorgchem.2c01109

Author Contributions

D.Z. spearheaded the experimental work including synthesis, characterization, and reactivity studies and wrote the paper. M.R.C. assisted with the collection and refinement of crystallographic data and helped with electrochemical measurements. A.N.O. assisted with experimental design. L.J.K. carried out porphyrin syntheses. S.N.M. contributed to crystallography data and refinement. T.R.C. designed the research and wrote the paper.

Funding

This work was supported by NSF CAREER Award #1847950 (T.R.C.). Characterization work was performed in part in the Chemistry Instrument Center (CIC), University at Buffalo, SUNY, Buffalo, NY. This work used the 12T Bruker SolariXR 12 Hybrid FTMS with Imaging MALDI and Nano-LC supported by NSF S10RR029517.

Notes

The authors declare no competing financial interest.

REFERENCES

(1) Jasinski, R. A New Fuel Cell Cathode Catalyst. *Nature* **1964**, *201* (4925), 1212−1213.

(2) Pegis, M. L.; Wise, C. F.; Martin, D. J.; Mayer, J. M. Oxygen Reduction by Homogeneous Molecular Catalysts and Electrocatalysts. *Chem. Rev.* **2018**, *118* (5), 2340−2391.

(3) Chen, R.; Li, H.; Chu, D.; Wang, G. Unraveling Oxygen Reduction Reaction Mechanisms on Carbon-Supported Fe-Phthalocyanine and Co-Phthalocyanine Catalysts in Alkaline Solutions. *J. Phys. Chem. C* **2009**, *113* (48), 20689−20697.

(4) Honda, T.; Kojima, T.; Fukuzumi, S. Proton-Coupled Electron-Transfer Reduction of Dioxygen Catalyzed by a Saddle-Distorted Cobalt Phthalocyanine. *J. Am. Chem. Soc.* **2012**, *134* (9), 4196−4206.

(5) Peljo, P.; Murtomäki, L.; Kallio, T.; Xu, H.-J.; Meyer, M.; Gros, C. P.; Barbe, J.-M.; Girault, H. H.; Laasonen, K.; Kontturi, K. Biomimetic Oxygen Reduction by Cofacial Porphyrins at a Liquid-Liquid Interface. *J. Am. Chem. Soc.* **2012**, *134* (13), 5974−5984.

(6) Collman, J. P.; Denisevich, P.; Konai, Y.; Marrocco, M.; Koval, C.; Anson, F. C. Electrode catalysis of the four-electron reduction of oxygen to water by dicobalt face-to-face porphyrins. *J. Am. Chem. Soc.* **1980**, *102* (19), 6027−6036.

(7) Chang, C. K. μ-Superoxodicobalt complex of a cofacial diporphyrin. *J. Chem. Soc., Chem. Commun.* **1977**, No. 22, 800−801.

(8) Collman, J. P.; Elliott, C. M.; Halbert, T. R.; Tovrog, B. S. Synthesis and characterization of 'face-to-face' porphyrins. *Proc. Natl. Acad. Sci. U. S. A.* **1977**, *74* (1), 18.

(9) Collman, J. P.; Wagenknecht, P. S.; Hutchison, J. E. Molecular Catalysts for Multielectron Redox Reactions of Small Molecules: The "Cofacial Metallodiporphyrin" Approach. *Angew. Chem., Int. Ed. Engl.* **1994**, *33* (15−16), 1537−1554.

(10) Collman, J. P.; Bencosme, C. S.; Barnes, C. E.; Miller, B. D. Two new members of the dimeric. beta.-linked face-to-face porphyrin family: FTF4* and FTF3. *J. Am. Chem. Soc.* **1983**, *105* (9), 2704−2710.

(11) Collman, J. P.; Marrocco, M.; Denisevich, P.; Koval, C.; Anson, F. C. Potent catalysis of the electroreduction of oxygen to water by dicobalt porphyrin dimers adsorbed on graphite electrodes. *Journal of Electroanalytical Chemistry and Interfacial Electrochemistry* **1979**, *101* (1), 117−122.

(12) Chang, C. K.; Liu, H. Y.; Abdalmuhdi, I. Electroreduction of oxygen by pillared cobalt(II) cofacial diporphyrin catalysts. *J. Am. Chem. Soc.* **1984**, *106* (9), 2725−2726.

(13) Chang, C. J.; Deng, Y.; Shi, C.; Chang, C. K.; Anson, F. C.; Nocera, D. G. Electrocatalytic four-electron reduction of oxygen to water by a highly flexible cofacial cobalt bisporphyrin. *Chem. Commun.* **2000**, No. 15, 1355−1356.

(14) Chang, C. J.; Loh, Z.-H.; Shi, C.; Anson, F. C.; Nocera, D. G. Targeted Proton Delivery in the Catalyzed Reduction of Oxygen to Water by Bimetallic Pacman Porphyrins. *J. Am. Chem. Soc.* **2004**, *126* (32), 10013−10020.

(15) Chang, C. J.; Deng, Y.; Heyduk, A. F.; Chang, C. K.; Nocera, D. G. Xanthene-Bridged Cofacial Bisporphyrins. *Inorg. Chem.* **2000**, *39* (5), 959−966.

(16) Deng, Y.; Chang, C. J.; Nocera, D. G. Direct Observation of the "Pac-Man" Effect from Dibenzofuran-Bridged Cofacial Bisporphyrins. *J. Am. Chem. Soc.* **2000**, *122* (2), 410−411.

(17) Cook, T. R.; Stang, P. J. Recent Developments in the Preparation and Chemistry of Metallacycles and Metallacages via Coordination. *Chem. Rev.* **2015**, *115* (15), 7001−7045.

(18) Cook, T. R.; Zheng, Y.-R.; Stang, P. J. Metal-Organic Frameworks and Self-Assembled Supramolecular Coordination Complexes: Comparing and Contrasting the Design, Synthesis, and Functionality of Metal-Organic Materials. *Chem. Rev.* **2013**, *113* (1), 734−777.

(19) Gao, W.-X.; Zhang, H.-N.; Jin, G.-X. Supramolecular catalysis based on discrete heterometallic coordination-driven metallacycles and metallacages. *Coord. Chem. Rev.* **2019**, *386*, 69−84.

(20) Barry, N. P. E.; Govindaswamy, P.; Furrer, J.; Süss-Fink, G.; Therrien, B. Organometallic boxes built from 5,10,15,20-tetra(4-pyridyl)porphyrin panels and hydroxyquinonato-bridged diruthenium clips. *Inorg. Chem. Commun.* **2008**, *11* (10), 1300−1303.

(21) Benavides, P. A.; Gordillo, M. A.; Yadav, A.; Joaqui-Joaqui, M. A.; Saha, S. Pt(ii)-coordinated tricomponent self-assemblies of tetrapyridyl porphyrin and dicarboxylate ligands: are they 3D prisms or 2D bow-ties? *Chem. Sci.* **2022**, *13*, 4070.

(22) Percástegui, E. G.; Jancik, V. Coordination-driven assemblies based on meso-substituted porphyrins: Metal-organic cages and a new type of meso-metallaporphyrin macrocycles. *Coord. Chem. Rev.* **2020**, *407*, 213165.

(23) Bar, A. K.; Chakrabarty, R.; Mostafa, G.; Mukherjee, P. S. Self-Assembly of a Nanoscopic Pt12Fe12 Heterometallic Open Molecular Box Containing Six Porphyrin Walls. *Angew. Chem., Int. Ed.* **2008**, *47* (44), 8455−8459.

(24) Oldacre, A. N.; Friedman, A. E.; Cook, T. R. A Self-Assembled Cofacial Cobalt Porphyrin Prism for Oxygen Reduction Catalysis. *J. Am. Chem. Soc.* **2017**, *139* (4), 1424−1427.

(25) Oldacre, A. N.; Crawley, M. R.; Friedman, A. E.; Cook, T. R. Tuning the Activity of Heterogeneous Cofacial Cobalt Porphyrins for Oxygen Reduction Electrocatalysis through Self-Assembly. *Chem.—Eur. J.* **2018**, *24* (43), 10984−10987.
(26) Crawley, M. R.; Zhang, D.; Oldacre, A. N.; Beavers, C. M.; Friedman, A. E.; Cook, T. R. Tuning the Reactivity of Cofacial Porphyrin Prisms for Oxygen Reduction Using Modular Building Blocks. *J. Am. Chem. Soc.* **2021**, *143* (2), 1098−1106.
(27) Han, Y.-F.; Lin, Y.-J.; Weng, L.-H.; Berke, H.; Jin, G.-X. Stepwise formation of "organometallic boxes" with half-sandwich Ir, Rh and Ru fragments. *Chem. Commun.* **2008**, No. 3, 350−352.
(28) Bruker. *APEX3*; Bruker-Nonius AXS, Inc.: Madison, WI, 2016.
(29) Sheldrick, G. SHELXT - Integrated space-group and crystal-structure determination. *Acta Crystallogr., Sect. A* **2015**, *71* (1), 3−8.
(30) Sheldrick, G. Crystal structure refinement with SHELXL. *Acta Cryst. C* **2015**, *71* (1), 3−8.
(31) Dolomanov, O. V.; Bourhis, L. J.; Gildea, R. J.; Howard, J. A. K.; Puschmann, H. OLEX2: a complete structure solution, refinement and analysis program. *J. Appl. Crystallogr.* **2009**, *42* (2), 339−341.
(32) *CrysAlisPRO*; Oxford Diffraction/Agilent Technologies UK, Ltd.: Yarnton, England.
(33) Kauffmann, M.; Roussel, P. New oxybromide cobaltites with layered perovskite-related structures: 18R-Ba6Co5BrO14 and 14H-Ba7Co6BrO17. *Acta Crystallographica Section B* **2007**, *63* (4), 589−596.
(34) Durand, R. R.; Bencosme, C. S.; Collman, J. P.; Anson, F. C. Mechanistic aspects of the catalytic reduction of dioxygen by cofacial metalloporphyrins. *J. Am. Chem. Soc.* **1983**, *105* (9), 2710−2718.
(35) Rosenthal, J.; Nocera, D. G. Role of Proton-Coupled Electron Transfer in O-O Bond Activation. *Acc. Chem. Res.* **2007**, *40* (7), 543−553.
(36) Liu, H. Y.; Weaver, M. J.; Wang, C. B.; Chang, C. K. Dependence of electrocatalysis for oxygen reduction by adsorbed dicobalt cofacial porphyrins upon catalyst structure. *Journal of Electroanalytical Chemistry and Interfacial Electrochemistry* **1983**, *145* (2), 439−447.
(37) Cai, Q.; Tran, L. K.; Qiu, T.; Eddy, J. W.; Pham, T.-N.; Yap, G. P. A.; Rosenthal, J. An Easily Prepared Monomeric Cobalt(II) Tetrapyrrole Complex That Efficiently Promotes the 4e-/4H+ Peractivation of O2 to Water. *Inorg. Chem.* **2022**, *61*, 5442.

https://doi.org/10.1021/acs.inorgchem.2c01109
Inorg. Chem. 2023, 62, 1766−1775